Fuel 282 (2020) 118506

Contents lists available at ScienceDirect

Fuel

journal homepage: www.elsevier.com/locate/fuel

Full Length Article

Development of biomass derived highly porous fast adsorbents for post-combustion CO_2 capture

Farooq Sher[a,*], Sania Zafar Iqbal[b], Shaima Albazzaz[c,d], Usman Ali[e], Daniela Andresa Mortari[f], Tazien Rashid[g,h]

[a] School of Mechanical, Aerospace and Automotive Engineering, Faculty of Engineering, Environmental and Computing, Coventry University, Coventry CV1 2JH, UK
[b] Department of Biochemistry, University of Agriculture, Faisalabad 38000, Pakistan
[c] Department of Chemical and Environmental Engineering, University of Nottingham, University Park, Nottingham NG7 2RD, UK
[d] Department of Chemical Engineering, College of Engineering, University of Basrah, Basrah, Iraq
[e] Department of Chemical Engineering, University of Engineering and Technology, Lahore 54890, Pakistan
[f] São Carlos School of Engineering, University of São Paulo (USP), São Carlos, SP, Brazil
[g] Department of Chemical Engineering, NFC Institute of Engineering and Fertilizer Research Faisalabad, Pakistan
[h] Department of Chemical Engineering, Universiti Teknologi Petronas, Bandar Seri Iskandar, Tronoh 32610, Perak, Malaysia

ARTICLE INFO

Keywords:
CO_2 capture
Biomass waste
Green activated carbons
Adsorption
KOH-activation
Microporous materials
Global warming

ABSTRACT

This study is carried out for a comparative screening of three groups of biomasses; soft or non-woody (peanut shell); intermediate woody (walnut shell) and hard woody (pine wood) for the development of adsorbents/activated carbons for post-combustion CO_2 capture (over N_2 balance). Three different groups of biomass residues are selected to study the role and nature of the material in adsorption and selection of the raw material for CO_2 adsorbents synthesis for future researches because of the hot issue of anthropogenic CO_2 emissions. The adsorption isotherms studied by the thermal gravimetric analyser (TGA) revealed that CO_2 adsorption capabilities are in the range of 2.53–3.92 mmol/g (over N_2 balance) at 25 °C. The newly synthesised activated carbons (ACs) exhibited a fast rate of adsorption as 41–94% in the initial 2 min. Porous surface development with catalytic KOH activation is seen clearly through SEM surface morphological analyses and mathematically confirmed from S_{BET} ranges from 146.86 to 944.05 m^2/g. FTIR and XRD peaks verify the generation of basic or inorganic O_2-rich moieties that help in acidic CO_2 capture. It has also been observed from adsorption isotherms that the order of higher adsorption groups is as; peanut shell > pine wood > walnut shell, while the best activation mass ratio (sample/KOH) is 1:3. The synthesised low cost ACs with an amount of 1.93 US$ per kg production could help to overcome the environmental hazards and problems caused by CO_2 and biomass waste.

1. Introduction

Because of the human activities, there is a noticeable increase observed in the warming of earth's atmosphere and expected to continue throughout the present century as of industrial development. This rapid progress of modern civilization is the primary cause of CO_2 emissions to the environment. Anthropogenic CO_2 from greenhouse gases is a main contributor to the global warming that is mostly discharged from fossil fuels combustion. Currently, the use of fossil fuels as an energy source continues to increase especially in developing countries, this is due to the availability of fossil fuels at a reasonable cost [1,2]. Literature confirmed the increment of > 30 billion tons of CO_2 to the atmosphere per year [3]. CO_2 emissions with this rate has upraised numerous alarms including urban smog, health issues as well as acid rain. Therefore, it is an urgent need of the hour to stabilise the level of this anthropogenic greenhouse pollutant (CO_2) before the extensive destruction. Consequently, in the presence of continuous climate change, the European Commission has decided to lessen its carbon discharge by 20–95% between 2020 and 2050 with reference to 1990 levels [4]. It is cleared in present energy setups of fossil fuels consumption, that the implementation of CO_2 capture and its storage (CCS) technologies could display an essential role to achieve the necessary reduction in CO_2 emissions to avoid irreversible and eternal destruction to the atmosphere [5–7].

At present, total three technologies have been introduced for CCS: pre-combustion capture, post-combustion capture and oxy-fuel combustion process. Post-combustion CSS technology can be simply retrofitted to the present-day power stations, petrochemical and gas

* Corresponding author.
E-mail addresses: Farooq.Sher@coventry.ac.uk, Farooq.Sher@gmail.com (F. Sher).

https://doi.org/10.1016/j.fuel.2020.118506
Received 2 January 2020; Received in revised form 11 April 2020; Accepted 21 June 2020

industries, oil refineries and cement industries, which worldwide accounts for nearly half of the CO_2 emissions [8,9]. Various separation techniques are available for post-combustion capture which includes absorption, cryogenic separation, adsorption and membrane [10,11]. The physical technique proved to be effective for the separation and purification of gas is adsorption. In adsorption technique, the solid sorbents used for capturing CO_2 have potential advantages over other conventional capturing treatment techniques including greater capacity, ease of handling, selectivity and reduced energy for regeneration.

However, adsorption method is costly, therefore, utilizing cheap materials for adsorbent preparation makes the method worthwhile. These materials include forestry wastes, agricultural residues and sewage sludge, the first two precursors have more carbon and very less ash content [12]. Different fruit stones, the by-products collected from food processing units are of special concern for obtaining carbon adsorbents with a better regular porous surface and appreciable hardness. Peach stones, apricot stones [13], olive stones [14], cherry stones [15] and grapestones [16] have been used as raw materials for the fabrication of activated adsorbents with high porosity and surface areas. Coconut shells have also been used for the fabrication of microporous adsorbents [17].

Activation of biomass is achieved by two methods; chemical activation and physical activation. The chemical activation method has some benefits over physical activation method. Firstly, it is a single step carbonization followed by activation with an activating agent and secondly, it is performed at a lower temperature as compared to physical activation [18]. The chemical activation procedure is associated with precursor material impregnation with activating agents (NaOH, KOH, $ZnCl_2$ or salts) then carbonized under inert pressure and finally washed to remove chemicals so that porous structure is left behind. Carbon adsorbents have been used for the treatment of industrial wastewater, removal of organic and inorganic pollutants from flue gases. In addition to its applications, the activated carbon is used as an adsorbent for CO_2 removal [12]. CO_2 adsorbents had been prepared from different starting materials other than biomass-based residues and by-products. A group of researchers prepared CO_2 adsorbents by KOH activation of petroleum pitch precursor [19]. The fabricated material exhibited an outstanding adsorption potential for CO_2 with values as high as 380 mg CO_2 /g sorbent at 0 °C temperature and 1 bar pressure. Nitrogen enriched CO_2 adsorbents have also been prepared from formaldehyde-urea resin by chemical activation with KOH [20]. For these nitrogen enriched activated carbons (ACs), the CO_2 adsorption limit is 1.40 mmol/g at 30 °C temperature under 12.5% CO_2 flow. Recently, a study is carried out to analyse the effects of CO_2 adsorption by ACs in terms of power loss and thermal efficiency. Upon comparison, it is concluded that ACs are more advantageous than the commercial adsorbents in rapports of cost and efficiency [21].

In the present study, different groups of biomass residues have been selected to study the role and nature of material in post-combustion CO_2 adsorption. The ACs have been prepared using biomass residues, therefore, this synthesis could be helpful in reducing landfill space to overcome the pollution and environmental issues caused by CO_2 emissions. The importance of this study over others is the diverse nature of biomass residues and their activation with a wide range of catalytic KOH. This research also identifies that which activation ratio is important in each group that is helpful for developing interesting surface chemistry, consistent morphology and porous surface structure with excellent surface parameters. The calculation of cost estimation for the production of per kg of ACs has also been performed in order to verify the cheapness of these adsorbents.

2. Experimental

Total twelve ACs have been prepared. The thermal gravimetric analyser (TGA) was used to study the CO_2 adsorption (over N_2 balance) of synthesised ACs. TGA results helped in the selection of the best samples from each group for further testing.

2.1. Synthesis of activated carbons

Biomass product; pine wood (PW) and by-products; peanut shell (PN) and walnut shell (NS) were selected as materials for the preparation of ACs. Pine wood was produced in Pakistan while the other two biomasses were obtained from a local market in the United Kingdom. First raw materials (PW, PS and WS) were crushed, then sieved to a particle size of 1 mm for further treatment. Potassium hydroxide (KOH) with 99% concentration (conc.) used as an activating agent was purchased from Sigma-Aldrich.

Biomass-based activated carbons (ACs) were prepared using a single-step chemical activation process, which can successfully develop potassium moieties on raw materials. In this protocol, 3 g of prepared raw material (PW, PN and NS) samples were first mixed physically with KOH (99% conc.) at different mass ratios including; 1:1, 1:2, 1:3 and 1:4 of raw sample/KOH (m/m). The physically mixed mixture (raw sample/KOH) was then heated in a horizontal tube furnace. The activation was carried out at 750 °C temperature with 5 °C/min heating rate in the presence of 1 L/min nitrogen flow [4].

When the reaction was reached to a specific temperature, the mixture was kept at this temperature for 1 h, before it was cool down in nitrogen (N_2) to ambient conditions. All the times, the neutral gas (N_2) was flowing inside the reaction furnace at 1 L/min flow rate. To get final products of ACs mixtures were removed from the furnace and cool down to room temperature then washed until neutral with distilled water (usually 3 times washing through 200 mL of water). The twelve synthesised activated carbons were labelled according to their precursor and mass ratio of activation agent are shown in Table 1.

2.2. CO_2 adsorption

CO_2 capture/adsorption measurements of ACs samples were carried out using thermogravimetric analysis (TGA Q500, TA Instruments USA). For individual measurements of CO_2 uptake, the sample was first dried at 120 °C in the presence of neutral N_2 gas for 1/2 h to eliminate any possible physisorbed CO_2 and/or the moisture content. Then the temperature was lowered to 25 °C for adsorption and stabilized. The reaction environment inside the reaction sample chamber was switched to flue gas (15% CO_2 in N_2) from N_2 at 100 mL/min flow rate at the

Table 1
Newly synthesised green activated carbons (ACs) with raw material and different ratio of the activating agent.

Sample ID	Composition	Mass ratio (sample: KOH)	Activation temperature (°C)
[a]NSK1	Walnut shell + potassium	1:1	750
[a]NSK2	Walnut shell + potassium	1:2	750
[a]NSK3	Walnut shell + potassium	1:3	750
[a]NSK4	Walnut shell + potassium	1:4	750
[b]PNK1	Peanut shell + potassium	1:1	750
[b]PNK2	Peanut shell + potassium	1:2	750
[b]PNK3	Peanut shell + potassium	1:3	750
[b]PNK4	Peanut shell + potassium	1:4	750
[c]PWK1	Pine wood + potassium	1:1	750
[c]PWK2	Pine wood + potassium	1:2	750
[c]PWK3	Pine wood + potassium	1:3	750
[c]PWK4	Pine wood + potassium	1:4	750

***Note: [a]NSK1, walnut shell sample activated with potassium in different m/m ratio; [b]PNK1, peanut shell sample activated with potassium in different m/m ratio; [c]PWK1, pine wood sample activated with potassium in different m/m ratio.

Table 2
Chemical analyses of raw biomass material samples.

Biomass samples	Ultimate analysis[a]							Proximate analysis[c]			
	C (%)	H (%)	N (%)	O[b] (%)	S (%)	H/C	O/C	M (%)	VM (%)	FC (%)	Ash (%)
Walnut shell	45.67	6.27	0.40	47.39	0.28	0.14	1.04	7.66	68.56	21.96	1.82
Peanut shell	46.34	6.42	1.95	45.07	0.23	0.14	0.97	6.45	71.87	17.50	4.18
Pine wood	44.78	6.17	0.42	48.38	0.26	0.14	1.08	6.97	72.54	17.07	3.47

M, VM, and FC value on dry basis except as denoted in the table.
a. Calculated by the difference.
b. On dry basis except moisture which is on as received basis.
c. As received basis.

above set adsorption's temperature for 1 h. The weight of final sample was noted to estimate the CO_2 uptake. CO_2 adsorption measurements were performed to analyze the ACs/adsorbents' surface affinity for CO_2 [22].

2.3. Characterisation

Ultimate analysis of the biomass samples was performed using a Flash EA 1112 elemental analyzer. Proximate analysis was obtained using the same TGA Q-500 instrument by heating the sample (s) from 10 to 110 °C/min in N_2 flow rate. These conditions were maintained for 10 min to obtain the moisture content. The temperature was then increased from 110 to 700 °C at 20 °C/min flow rate (under N_2) and kept for 30 min at these conditions to get the weight loss due to devolatilisation after this temperature was ramped at the same rate to 950 °C/min. The reaction environment was then switched from N_2 to air, inside the furnace compartment and kept it isothermal for 40 min to oxidise the char completely to obtain the fixed carbon and ash contents [23]. The results of different weight percentages of fixed carbon (FC), ash, volatile matter (VM), carbon (C), nitrogen (N), hydrogen (H) and oxygen (O) of raw precursors (PN, NS, and PW) are presented in Table 2.

Micromeritics ASAP 2420 instrument was used for surface textural parameter measurements of the prepared ACs with N_2 uptake of the ACs at 77 K. The ACs were degassed first at 120 °C temperature for 16 h before micromeritics measurements. The specific surface area (S_{BET}) was calculated by standard Brunauer–Emmett–Teller (BET) method utilising N_2 isotherm adsorption data within 0.01 to 0.1 relative pressure range. The adsorbed quantities of N_2 at P/P_0 of ca. 0.99, were used for the calculation of total or cumulative pore volumes (V_{total}). Average pore diameter was determined using $4V_{total}/S_{BET}$ [24].

The volume of micropore (V_{micro}), was estimated by t-plot method. Total mesopore volume V_{meso} obtained by subtracting the micropore volume from the total pore volume [25]. Then the micro porosity percentage of the selected ACs was calculated by V_{micro}/V_{total}. Similarly, the mesoporosity percentage was calculated using V_{meso}/V_{total}. Crystallographic analyses of the synthesised carbons before and after activation were inspected with the help of D8 Advance XRD diffractometer (Bruker Inc., Germany) and Cu Kα radiation source. While the values of voltage and current used for XRD experiments were 40 kV and 40 mA respectively.

Organic moieties generated on the surface of ACs were characterised by Fourier Transform Infrared (FTIR) Spectroscopy (Bruker Vertex 70 spectrometer) [26]. For FTIR investigations sample pellets were prepared with potassium bromide salt. The spectras were noted in between 400 and 4000 cm^{-1} wave number range. A mortar was used to ground 0.0015 g sample with 0.25 g of KBr. The obtained powder was then placed under a mechanical pressure of 10 kPa/mm^2 in a circular die for 10 s. After this, the sample was transferred to an oven for drying at 100 °C for 48 h under vacuum to avoid any interface between the mix, CO_2 molecules and water vapours. The temperature was reduced to room temperature under vacuum overnight. At the last, the sample was transferred to the analyser.

Surface morphology of all the raw samples as well as the best performing ACs derived from these samples were obtained by using a scanning electron microscope (SEM) instrument (JEOL 7100F FEG-SEM) at 15 kV. Between three and four repeat runs for each experiment were performed to ensure appropriate repeatability and validity of the results.

3. Results and discussion

3.1. Evaluation of CO_2 capture performance

The CO_2 adsorption (over N_2 balance) isotherms of twelve fabricated ACs (Table 1) are plotted in Fig. 1 to Fig. 3. Adsorption kinetics were determined from TGA as a function of time at 25 °C temperature. These CO_2 adsorption isotherms shown a remarkable CO_2 uptake capacity of ACs ranging from 2.53 to 3.92 mmol/g. While the lower range of CO_2 (over N_2 balance) uptake (2.53 mmol/g) of this study is comparable to other ACs synthesised from phenolic resins [27] and rice husk waste [4]. The phenolic resin based carbons were activated with different ratio of HNO_3 while rice husk carbons were activated with different KOH ratio. In both of these previous studies, CO_2 adsorption was not > 2 mmol/g. The synthesised ACs derived from three different biomass precursors (NS, PN and PW), each biomass sample was reacted with four different ratios of KOH. Therefore, four different ACs (NSK1, NSK2, NSK3 and NSK4) were synthesised from walnut shell biomass only. Treatment with KOH changes the textural properties and chemical nature of functional groups of precursors. Activation with different mass ratios of KOH strategy was applied to prepare K-ACs with high porosity, surface area and increased amount of basic oxygen

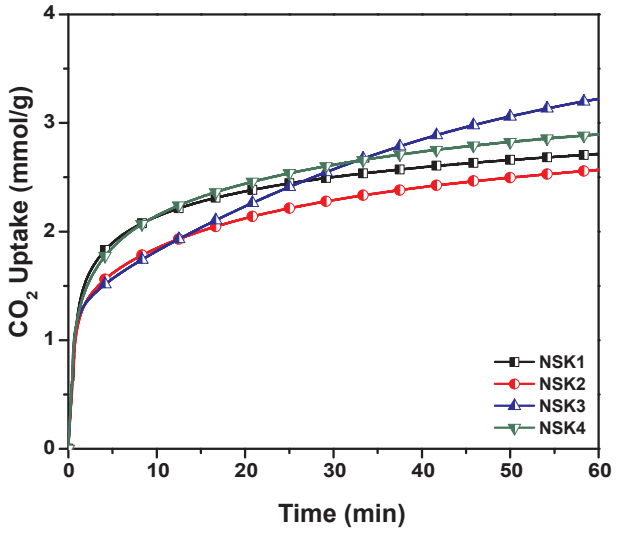

Fig. 1. CO_2 uptake isotherms of walnut shell (NS) derived ACs at 25 °C.

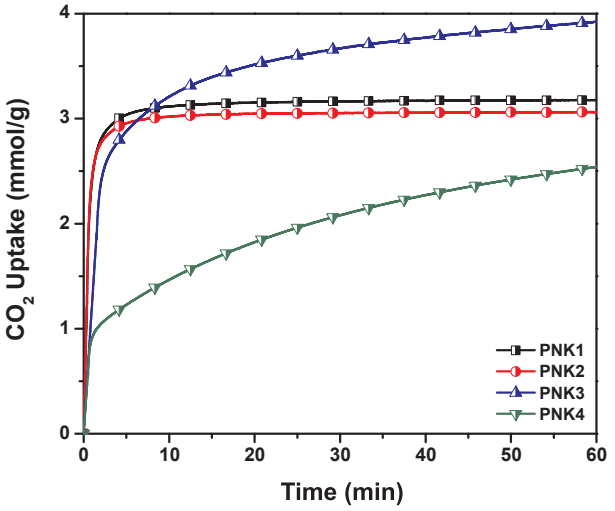

Fig. 2. CO_2 uptake isotherms of peanut shell (PN) derived ACs at 25 °C.

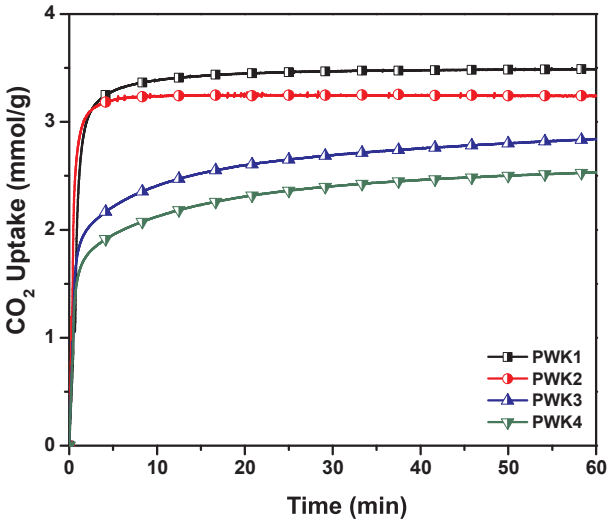

Fig. 3. CO_2 uptake isotherms of pine wood (PW) derived ACs at 25 °C.

functionality, all these factors helped in higher CO_2 uptake. This activation strategy with different KOH rations was also proved to be beneficial from previous researches [28]. Higher amount of KOH helps in the generation of more porous structures followed by high CO_2 uptakes, this can be confirmed from Fig. 1, as different KOH amount yields different CO_2 uptake these results are in accordance with Singh, G., et al., [28].

The CO_2 uptake of 3.23 > 2.90 > 2.71 > 2.57 mmol/g were noted for walnut shell derived different ACs NSK3 > NSK4 > NSK1 > NSK2 respectively as shown in Fig. 1. These values are reported by rounding off the digits up to two decimal places. Similarly, 3.92 > 3.18 > 3.06 > 2.54 and 3.49 > 3.24 > 2.84 > 2.53 mmol/g uptakes were measured for peanut shell samples: PNK3 > PNK1 > PNK2 > PNK4 (Fig. 2), and pine wood samples: PWK1 > PWK2 > PWK3 > PWK4 (Fig. 3) respectively. The best activated carbon from the walnut shell is NSK3, from peanut shell is PNK3 and from pine wood biomass is PWK1.

Comparatively, from three groups the most highly activated carbon is PNK3 and least one is PWK4. In the case of walnut shell ACs, 3.23 mmol/g of CO_2 adsorption peak was noticed, while the overall CO_2 adsorption is 60% in initial 4 minutes after that it was increased constantly with time for 1 h. Similar trends were noticed for other carbons in the same time interval. Up to 16 min NSK4 showed a higher rate of uptake, but after that NSK3 exhibited a sudden increase in CO_2 uptake and goes on increasing up to 60 min. The CO_2 uptake capacity of different walnut shell ACs is different and increased little by increasing the mass ratio of KOH (KOH/sample) up to 3:1. Beyond this combination, further increase in the amount of activating agent did not increase the CO_2 uptake of the activated carbon (Fig. 1). For NSK4 the CO_2 uptake is lowered to some extent as compared to NSK3 that could be because of the lower number of adsorption, active and suitable functional group sites.

For peanut shell derived ACs, 3.92 mmol/g CO_2 adsorption peak was noticed while the overall CO_2 adsorption is equivalent to 80% in initial 3 to 4 min. After this initial 80% adsorption capacity, horizontal plateaus of adsorption isotherms were observed for PNK1 and PNK2 indicating the saturation of available microspores (Fig. 2). A constant increase of adsorption with time was observed for PNK3 also illustrates from its blue isotherm (Fig. 2). However, for PNK4 a decrease in adsorption capacity was observed that was similar to NSK4 isotherm. Likewise, for pine wood derived ACs, the peak value of 3.49 mmol/g for CO_2 adsorption was observed. The overall CO_2 adsorption is equivalent to 91% in initial 2 to 3 min followed by somewhat horizontal plateaus of adsorption for PWK1 and PWK2 [4]. While for PWK3 and PWK4 relatively lower adsorptions were noticed that could be because of a decrease in porosity with an increase in KOH activation (Fig. 3).

Physisorption carbons with porous surfaces have reasonably fast kinetics [29]; comprise diffusional transports in micro and macropores. That's why this study is designed on the physisorption principle (CO_2 uptake). All these CO_2 adsorption kinetics results in association with different KOH mass ratios concluded that the best group that has shown fast CO_2 uptake rates is PW derived ACs, while the group for higher CO_2 adsorption capacity is PN derived ACs (Fig. 4). The adsorption amount reported with TGA is CO_2 adsorption over N_2 balance rather than pure CO_2 adsorption [4], because flue gas comprises of 15% CO_2 with N_2 [30]. It is observed that CO_2 adsorption capacities of ACs are higher than N_2 but in parallel N_2 adsorbs little with CO_2 in flue gas analysis. While the amount of N_2 is reported usually less or equals to 0.5 mmol/g [31].

3.2. Textural analysis of activated carbons

N_2 adsorptions were performed for six samples (Fig. 5) out of twelve among which three were those exhibited higher CO_2 uptake (PNK3 > PWK1 > NSK3). The other three selected ACs were those either the least adsorbed carbon (PNK4) from a particular group of ACs with higher KOH ratio or the carbon with relatively higher CO_2 uptake but

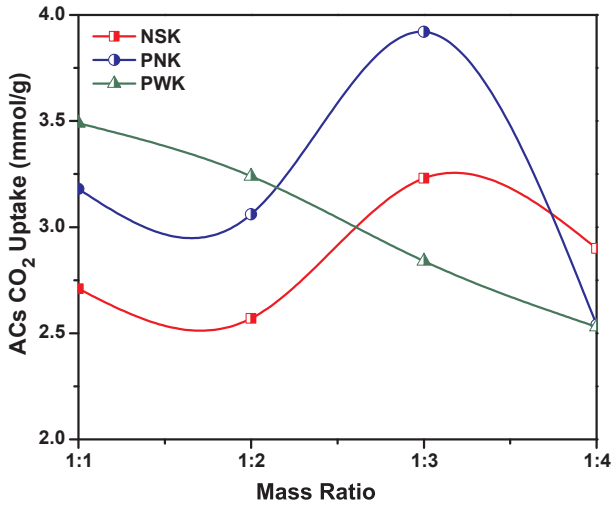

Fig. 4. The role of KOH in CO_2 uptake for adsorbents synthesised from different biomasses.

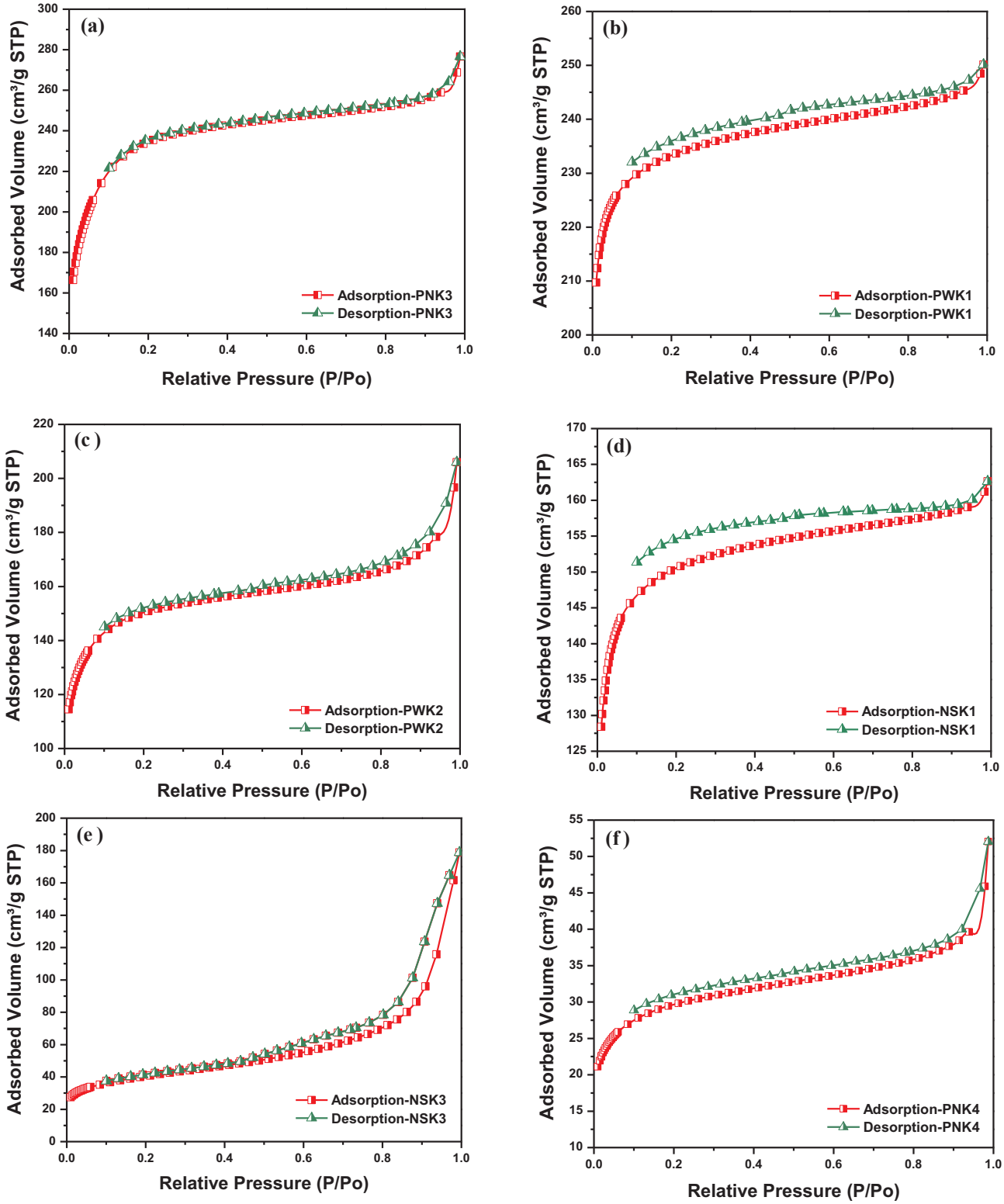

Fig. 5. N_2 adsorptions isotherms of selected ACs; peanut shell group (a and f), pine wood group (b and c) and walnut shell group (d and e).

with least ratio of KOH (NSK1) from another group of ACs. The effect of porosity on the adsorption of N_2 is shown in the form of N_2 adsorption isotherms. Surface textural and pore structure calculations obtained from the BET measurements are incorporated in Table 3. It can be seen that V_{total} and S_{BET} increased from 0.07 to 0.38 cm^3/g and 112.33 to 944.05 m^2/g respectively for different ACs fabricated at 750 °C and 0.15 bar pressure. It is cleared that the ACs derived from KOH activation protocol are microporous with the microporosity accounting for up to 95% of the total porosity.

The N_2 sorption (adsorption and desorption) isotherms of PNK3, PWK1, PNK4, NSK1 and PWK2 are found similar to Type I isotherm that is also verified from the International Union of Pure and Applied Chemistry (IUPAC) data sources [32]. While one of the selected samples, NSK3 has shown Type II isotherm. Literature confirms that N_2

Table 3
Surface and pore structure statistics of ACs measured from N_2 sorption.

Sample	S_{BET} (m^2/g)	V_{total} (cm^3/g)	Average pore diameter (nm)	V_{micro} (cm^3/g)	$V_{meso} = V_{total} - V_{micro}$ (cm^3/g)	Microporosity $= V_{micro}/V_{total}$ (%)	Mesoporosity $= V_{meso}/V_{total}$ (%)
PNK3	900.76	0.38	1.69	0.33	0.05	87	13
PNK4	112.33	0.07	2.49	0.04	0.03	57	43
NSK1	603.25	0.22	1.46	0.21	0.01	95	5
NSK3	146.86	0.26	7.08	0.04	0.22	15	85
PWK1	944.05	0.35	1.48	0.33	0.02	94	6
PWK2	581.07	0.29	1.99	0.21	0.08	72	28

sorption Type I isotherms are obtained for those adsorbents having very small pores usually known as micropores. The presence of these micropores verifies from sharp N_2 uptake capacity of PNK3, PWK1, PWK2 and NSK1 adsorbents at low pressure $<$ 0.1 bar. Afterwards, the development of horizontal plateaus at higher pressures attributed to an extraordinary microporosity of these selected ACs ranges from 72 to 95%. These results provide the reasons for higher CO_2 uptake and fast adsorption kinetics of the above mentioned ACs. Comparatively at further higher pressures variable minor to significant hysteresis loops are observed for PWK1, NSK3, PNK4, PWK2 and NSK1. Hysteresis loop suggests the presence of mesoporous surface of adsorbent at these pressures generated by the gas condensation [22]. While Type II N_2 adsorption isotherm shown by the adsorbent NSK3 indicates mesoporous surface with 15% microporosity.

Higher specific surface area and micropores volume of PNK3, higher adsorption capacities of NSK3 and PWK1 derived ACs support the variable amount strategy of KOH used for activation from minor (1:1) to significant (1:4) range is successful. Increase in micropores volume and surface area is detected because of oxidation and gasification reactions proceed via decomposition of potassium carbonate (K_2CO_3) at a high temperature that is also supported with SEM images.

The lower S_{BET} of two selected ACs; NSK3 $>$ PNK4 is 146.86 $>$ 112.33 m^2/g. This decreasing order of S_{BET} is observed with an increasing ratio (1:3 to 1:4) of the activating agent in the synthesised ACs. This might be because of the over oxidation of carbons and development of insoluble potassium (K) residues. The relatively lower S_{BET} obtained for activated carbons was because of K impregnation that led to fractional or even thorough occlusion of pores. Therefore, a peak concentration of potassium is observed, above that the additional residual potassium (PNK4) helps little to capture CO_2. This discussion confirms that the overall best ratio among all 12 fabricated ACs derived from three different groups of precursors is 1:3 (sample: KOH) because on further activation with KOH leads to over oxidation and formed macro-pores credited to adsorption of 2.54 mmol/g of CO_2 uptake. From Table 3, it could be verified that the BET measurements for these adsorbents are consistent with their Type I (Fig. 5f) and Type II (Fig. 5e) isotherms [33]. Fig. S1 shows an observed comparative analysis of N_2 adsorbed volumes of the selected ACs. Furthermore, it is seen that the volume of N_2-adsorbed for PNK4 is very small owing to its relatively lower developed total pores Vt_{otal}.

The presence of different pores sizes in selected ACs from each group are comparatively illustrated in Fig. 6. In the case of PNK3, PWK1 and PWK2 three different pores sizes have been generated; micropores/mesopores ($<$ 50 nm) and macropores ($>$ 50 nm). While in the case of NSK1, NSK3 and PNK4 most probably generated pores are $<$ 50 nm in size. Among these, more are mesopores (2–50 nm) while some are micropores ($<$ 2 nm). Fig. S2 investigates the bimodal pore structure and its development by KOH activation of the best performing ACs from different groups. Fig. S3 shows an observed dependence of CO_2 uptake on the developed pore volume by KOH treatment.

3.3. KOH intercalation mechanism

Type I isotherms Fig. 5(a-d, f) are observed because KOH

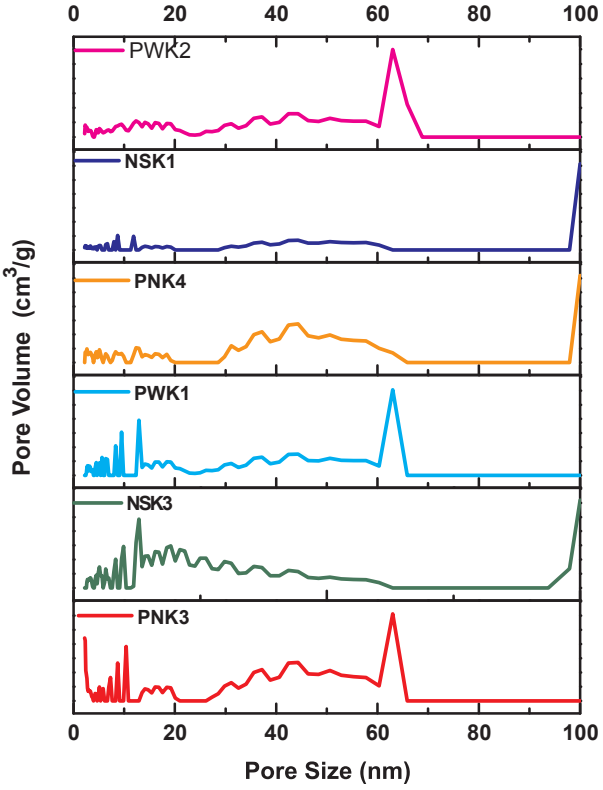

Fig. 6. Pore size distribution for selected samples from different groups of biomass.

impregnation acts as a catalyst to speed up the gasification reaction as mentioned in equations ((2) to (5) and (6)) [32,34]. Reaction intermediates K_2CO_3 and K_2O are formed at a temperature $>$ 700 °C. These polar/basic intermediates react with the carbon matrix to fabricate a framework with micropores. The carbon framework development from non-porous to porous upon treatment with KOH is also confirmed by SEM analyses.

Polymeric components present in biomass undergo different chemical reactions including cracking, aromatisation, dehydration, dehydrogenation and depolymerisation during carbonisation process followed by treatment with KOH base [28]. The later reaction is applied to activate the carbon matrix through a series of reactions (1 to 8). The redox reaction of biomass carbon with KOH leads to oxidation of carbon matrix that yields potassium carbonate (K_2CO_3) and hydrogen (H_2) gas (reactions (2)–(4)). The oxidation process and resultantly the presence of oxidised species on the surface of ACs are in agreement with relevant FTIR peaks in the developed oxidised functional group region (1000–1860 cm^{-1}).

$$2KOH \rightarrow K_2O + H_2O \quad (1)$$

$$C + H_2O \rightarrow CO + H_2 \quad (2)$$

$$CO + H_2O \rightarrow CO_2 + H_2 \quad (3)$$

$$CO_2 + K_2O \rightarrow K_2CO_3 \quad (4)$$

$$K_2CO_3 \rightarrow K_2O + CO_2 \quad (5)$$

$$CO_2 + C \rightarrow 2CO \quad (6)$$

$$C + K_2O \rightarrow C\text{-}O\text{-}K + K \quad (7)$$

$$C + K_2O \rightarrow 2\,K + CO \quad (8)$$

Progressively, as temperature arose the chemicals/functional groups of biomass decompose and gasification occurs (reactions (5), (6) and (8)), rest of the mass forms char through aromatisation reaction. The presence of aromatic groups after activation is observed from the FTIR peaks of activated carbons in the related fingerprint region (808–893 cm^{-1}). Gasification/or escape of volatile components cause the development of porous surface from non-porous carbon framework/matrix [20].

The biomass carbon reacts with the KOH until it is consumed completely and as a result converted into metallic K and other volatiles. K_2CO_3 formed, further reacts with carbon (biomass) to generate K_2O, K and volatiles (reactions (4) to (8)). The development of high porosity is credited to the reactions ((2) to (8)) of dehydration, polymerisation and evolution of gases. Potassium based compounds formed (reaction (7)) during the activation process are well intercalated/or impregnated into the carbon framework. While later the removal of these compounds (K species) using water treatment results in the fabrication of porous surfaces of ACs [32]. Therefore, it can be said that the possible effect of KOH treatment on the studied carbons was porosity generation with well observed gasification reactions.

3.4. Crystalline surface analysis

The synthesised CO_2 adsorbents have also been studied for their microcrystalline or amorphous nature by powdered XRD patterns (Fig. 7). These analyses were applied to a selected number of activated (NSK1, NSK3, PNK3, PNK4, PWK1 and PWK2) and corresponding non-activated carbons (NS, PN and PW) to identify the changes on the surface of adsorbents before and after activation. The peak intensities in the case of activated carbons and non-activated carbons are in exact accordance with the KOH ratios. In case of all non-activated and some activated carbons, one broad and two weak peaks have been noticed around 2θ = 22–25°, 43° and 45°. A broad peak of quite high intensity around 22–25° is observed for NS, PN and PW carbons that confirms the amorphous nature of non-activated carbons. This peak around 22–25° is identical to (0 0 2) diffraction of graphite and confirms the hexagonal nature of NS, PN and PW carbons. While the two weak peaks around 2θ = 43° and 45° corresponded to the (1 0 1) and (1 0 0) diffraction planes of graphite are observed in relation to their partial microcrystalline nature [4].

A clear shift in XRD peaks has been observed for activated carbons in comparison to non-activated carbons of all groups. In case of walnut shell derived activated carbon NSK1 relatively less intense peaks are detected around 25°, 43° and 45°. The peak (0 0 2) diffraction plane of graphite is absent in case of NSK3 in comparison to raw non-activated carbon NS. The absence of this characteristic peak might be due to the collapse of carbon matrix. The encircled area sharp peaks of NSK3 may be attributed to the development of more chemical species in the interlayers of collapse hexagonal graphite (carbon). Likewise, in the case of peanut shell derived ACs, again interesting surface chemistry has been confirmed from XRD patterns. Broad peaks around the characteristic range of 22–25° and 43° in the case of non-activated PN are developed into sharp ones for PNK3 because of increasing KOH ratio. It is also observed from XRD pattern that sample/KOH ratio of 1:4 is not helpful in the activation of carbons because in the case of PNK4, the peaks almost disappeared in comparison to PNK3 and PN. The intensity

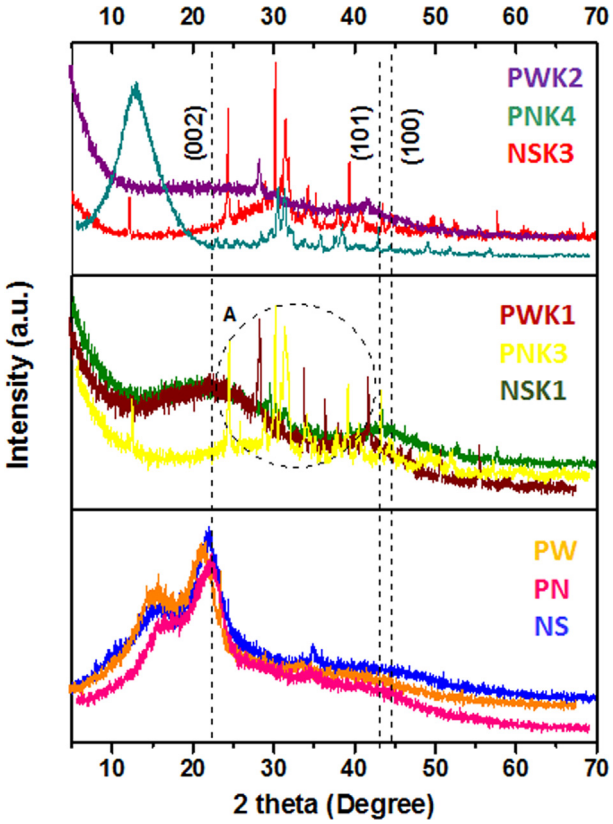

Fig. 7. XRD profile of walnut shell, peanut shell and pine wood derived non-activated precursor and activated carbons.

of the observed peaks is also lowered in comparison to 1:3 and 1:2 ratios. This type of behaviour might be noted as of destructive interferences developed because of a relatively high amount of KOH [20]. This destructive interference of KOH might cause the degradation of porous structures. Moreover, XRD profiles of pine wood group are exactly similar to the peanut shell group. The peak centred around 26° to 27° is noticed for the generation of inorganic crystalline compounds [35].

3.5. Surface chemistry analysis

FTIR analyses were performed for six samples. Three were non-activated carbons: NS, PN and PW and three activated carbons: NSK3, PNK3 and PWK1. In the case of walnut shell based non-activated carbon NS; the presence of peaks at 3664 (O–H str), 3263 (N–H str), 2467 (O–H str), 1857 (C═O str), 1660 (C═O str), 1463, 1326 (O–H def) and 690 (CH def) cm^{-1} correspond to OH, NH or might be chelate, carboxylic acid, carbonyl group of quinone, α-β unsaturated ketone, methyl, alcohol and alkenyl groups respectively (Fig. 8). However, NSK3 spectra confirms its activation and graphitisation that is also verified with the similar results obtained from XRD profiles of this material. The peaks of NSK3 at 3664 (O–H str), 3263 (N–H str), 2397, 1774 (C═O str), 1620 (C═O str), 1458 (C═C), 1344 (O–H def), 1120 (C-O str), 808 (CH def) and 617 (CH def) cm^{-1} indicate the generation of OH, NH/or might be chelate, carboxylic acid, ester, carbonyl group with benzene, double bond of aromatic ring, alcohol, ether, *p*-substituted aromatic ring and alkenyl groups respectively (Fig. 8). Like in NSK3, almost similar type of functional groups were developed on the surface of PNK3 after activation that might be because of the same mass ratio of the activating agent.

The presence of peaks at 3691 (O–H str), 2891 (CH str), 2380, 1832 (C═O), 1645 (C═O str), 1450 (def), 1249 (C-O str) and 640 (def) cm^{-1} correspond to OH, aldehyde, carboxylic acid, carbonyl of anhydride,

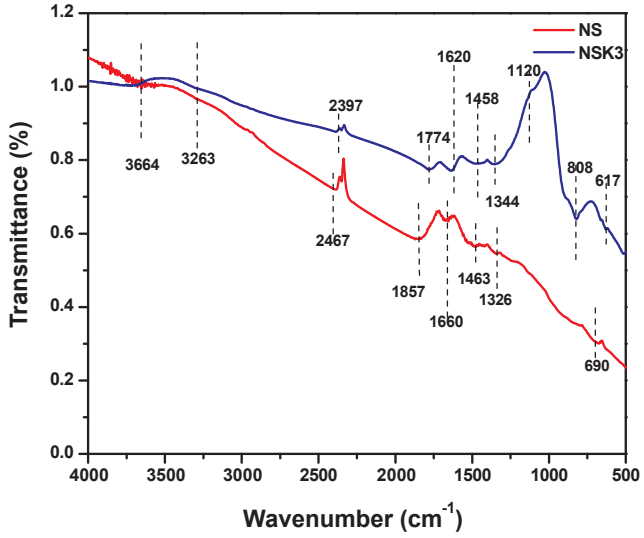

Fig. 8. FTIR spectra of walnut shell derived non-activated precursor and activated carbon.

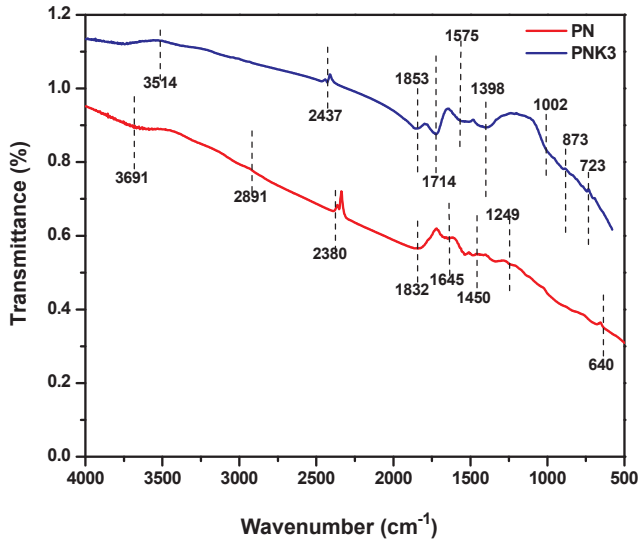

Fig. 9. FTIR spectra of peanut shell derived non-activated precursor and activated carbon.

carbonyl of diaryl ketone, methyl, diaryl ether and CH groups respectively in the case of PN non-activated carbon (Fig. 9). This precursor on activation with KOH in 1:3 ratio fabricated PNK3, its FTIR spectra confirms its activation. Furthermore, these FTIR results are also supported with SEM results of the respective AC. The peaks of PNK3 at 3514 (O–H str), 2437, 1853 (C═O str), 1714 (C═O str), 1575 (N–H def), 1398 (O–H def), 1002 (C-O str), 873 (CH def) and 723 (rocking *v*) cm^{-1} correspond to dimer or chelate, carboxylic acid, carbonyl of anhydride, carbonyl of diaryl ketone, aromatic amine, phenol, ether, substituted aromatic ring and CH groups respectively (Fig. 9).

Likewise, for PW precursor the bands at 2314, 1799 (C═O str), 1672 (C═O str), 1471 (def) and 779 (CH def) cm^{-1} correspond to carboxylic acid, carbonyl of acid halide, carbonyl of diaryl ketone, CH3, *m*-disubstituted aromatic group, while PWK1 with 1:1 KOH/sample ratio indicated bands at 3683 (O–H str), 2351, 2250 (str), 1814 (C═O), 1635 (N–H def), 1469, 1315 (C-O),1112 (C-O str), 893, 798 and 657 cm^{-1} attribute to free OH, carboxylic acid, alkenyl, carbonyl of acid halide, secondary amine, alcohol, C-O of anhydride, ether, two bands for weak and strong *m*-disubstituted aromatic ring and CH groups respectively (Fig. 10). The presence of dimers, chelates and

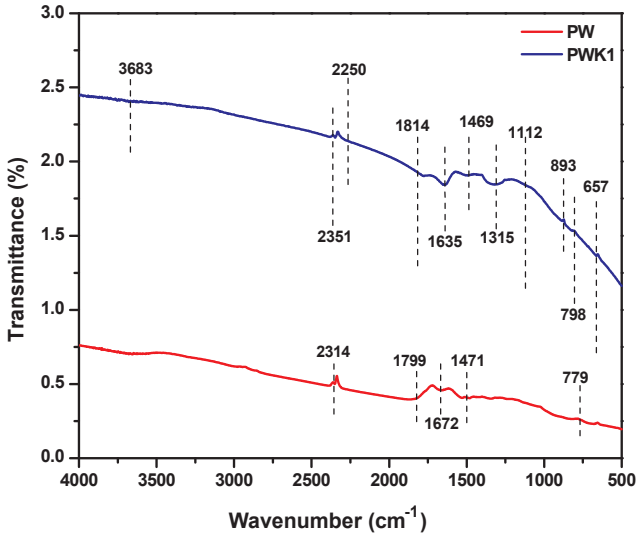

Fig. 10. FTIR spectra of pine wood derived non-activated precursor and activated carbon.

disubstituted aromatic ring in the case of PNK3, NSK3 and PWK1, confirms the aromatisation reactions with KOH impregnation. The developed basic groups of ACs help in the adsorption of acidic CO_2 because of electrostatic interactions developed between them at a higher temperature (reaction (7)).

3.6. Surface morphology analysis

The morphological analyses were carried out for non-activated (NS, PN and PW) precursors and the best performed ACs including; NSK3 from NS, PNK3 from PN and PWK1 from PW. These ACs not only showed higher CO_2 uptake in their groups but also confirmed with FTIR spectra, their modified surface chemistries in comparison to their non-activated forms as a result of activation. Walnut shell based non-activated precursors NS shows non-porous and flat morphology in comparison to their activated form NSK3 as illustrated in (Fig. 11). SEM images of NSK3, clearly show changed surface morphology than precursor not showing more microspores. Additionally, the pore diameter of NSK3 is seen much larger than other porous ACs; PNK3 (Fig. 12d) and PWK1 (Fig. 13b).

Moreover, it could reasonably be said that the decomposition of carbon matrix/walls of NSK3 connecting porous structure via high content of KOH took place. Carbon walls oxidised at high temperature 750 °C, generated K residues that change its morphology completely. Therefore, it could be concluded that NSK3 revealed a carbon matrix collapse with a higher mass ratio of KOH. Sometimes, if the higher CO_2 capture of activated carbons (K-ACs) cannot be compatible with surface textural features then porosity decreases with activation. Then in such cases, the higher CO_2 uptake of K-ACs attributes to modified surface chemistries [28]. In the case of NSK3 potassium intercalation instead of relatively lower microporosity plays a key role in CO_2 capacities. Therefore, it could be said that the polarized surface functional groups are helpful to enhance surface interaction with quadrupole moment of CO_2 and consequently instigated higher CO_2 uptake [28].

The SEM images of non-activated peanut shell derived precursor PN showed a flat non-porous surface and developed into a highly porous surface (PNK3) on treatment with an activating agent as illustrated in Fig. 12. Removal of gases during the process of activation according to redox stoichiometric equations ((5) to (6) and (8)) were credited to a flat, regular and 87% microporosity of PNK3 [20]. These pores justify more diffusion/or adsorption of CO_2 from bulk to the adsorbent (PNK3) surface. Porosity generation phenomenon was also observed similar to the peanut shell in pine wood group. There is a clear difference between

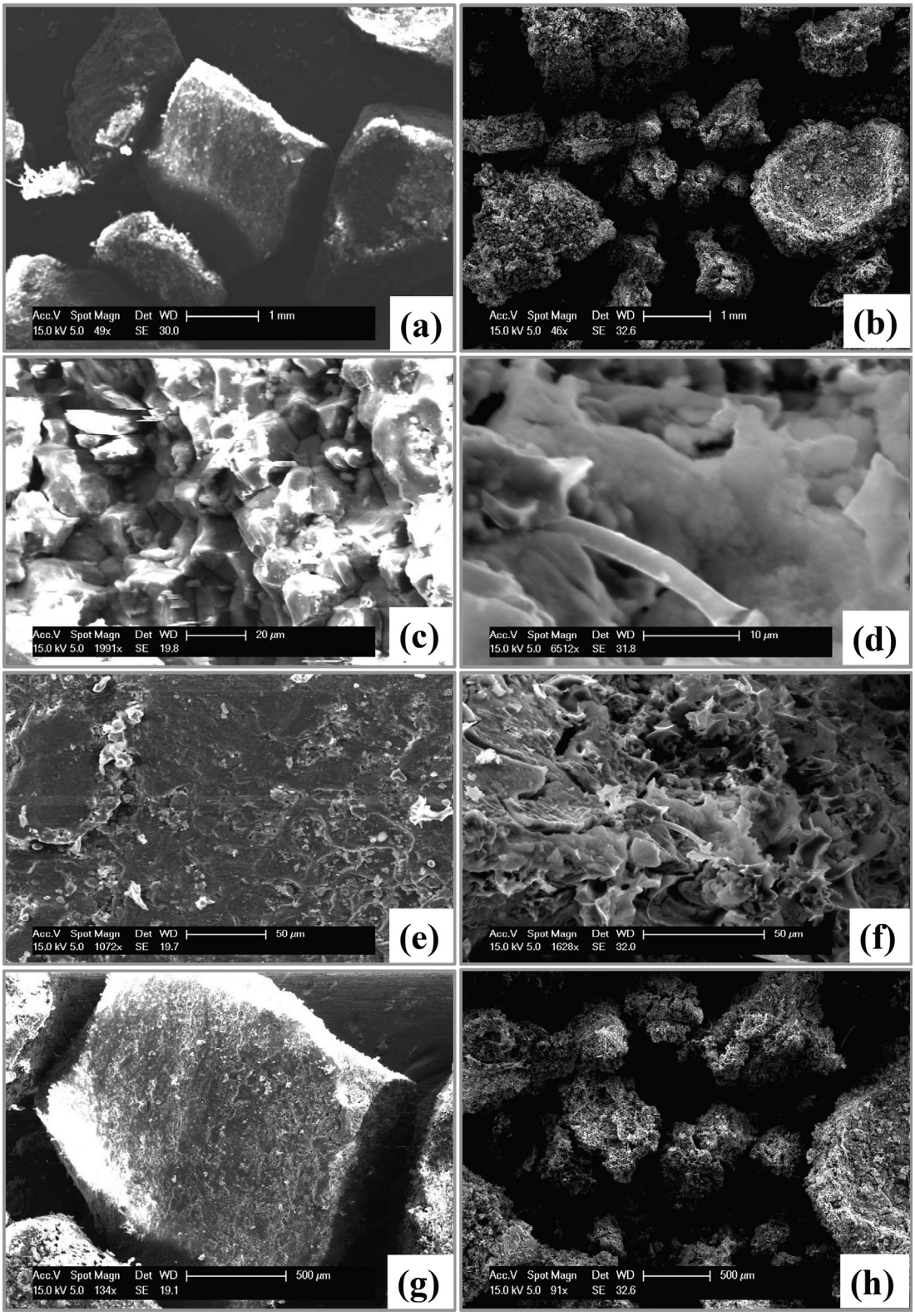

Fig. 11. SEM analysis of walnut shell derived non-activated; NS (a, c, e and g), and activated carbons; NSK3 (b, d, f and h).

the morphological surfaces of PW, PWK1, non-activated and activated forms of pine wood precursor and carbon respectively as shown in Fig. 13.

3.7. Fast adsorption potential

CO_2 adsorption (over N_2 balance) measurements for the first 120 s have been reported for activated carbons. The CO_2 uptake measurements of adsorbents in the first 120 s in comparison to 1 h verified that the developed ACs are very responsive and free from time dependent

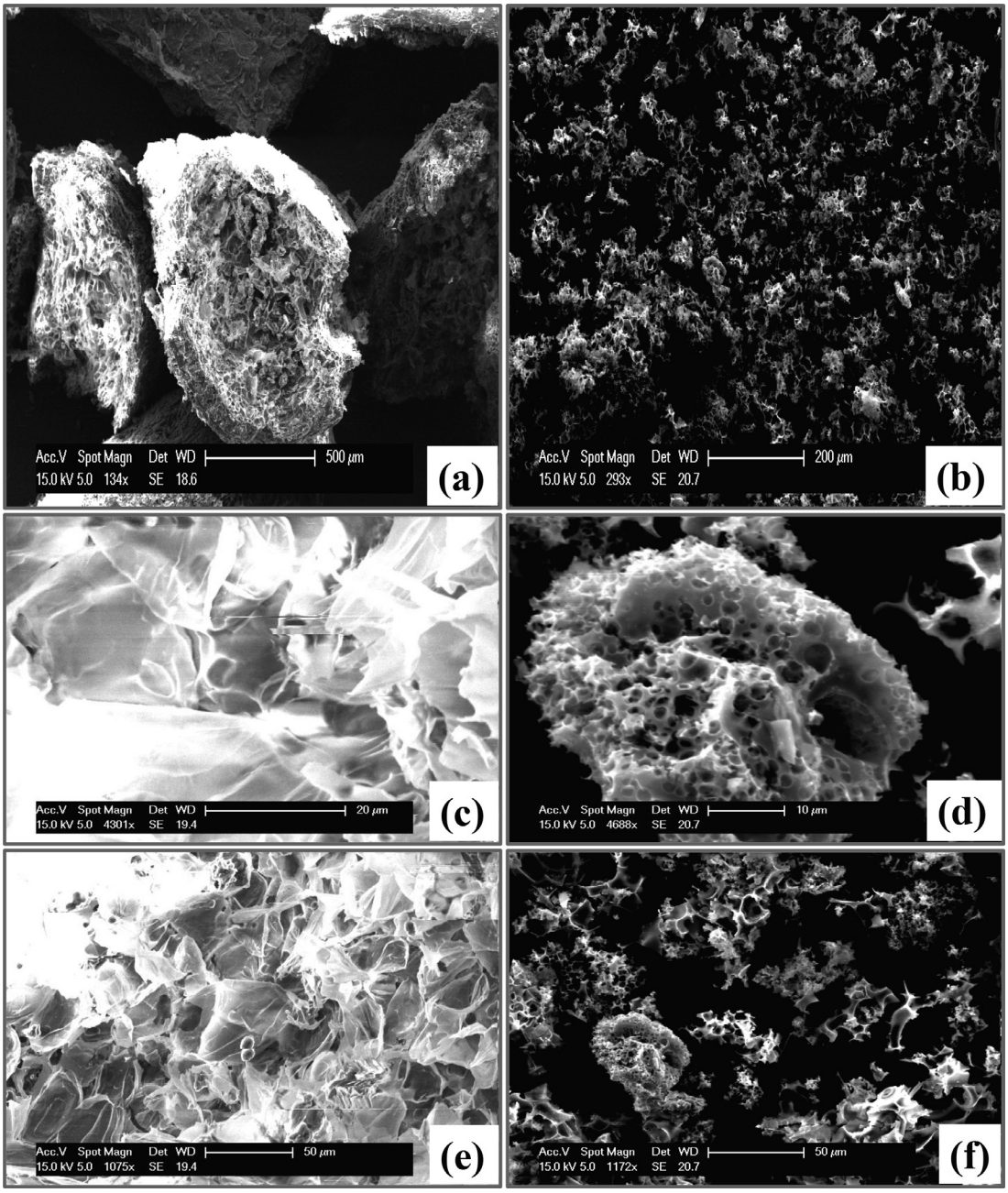

Fig. 12. SEM analysis of peanut shell derived non-activated; PN (a, c and e), and activated carbons; PNK3 (b, d and f).

factor to much extent. From Table 4, it could be observed that almost all adsorbents with one or two exceptions showed an average > 60% uptake of CO_2 from total in the first 120 s. In the case of walnut shell derived ACs (Fig. S4(a)) the CO_2 uptake in first 120 s is 50% in average, which is 20% lower than peanut shell derived ACs (Fig. S4(b)) and 30% lower than pine wood derived ACs (Fig. S4(c)). The possible reason behind this could be the different composition and diverse nature of the material. Moreover, PNK2 and PWK2 have presented an ideal case by adsorbing > 90% of CO_2 from the total in first 120 s. Under the current scenario of environmental pollution [36,37], there is a need to develop renewable fuels [38] and sustainable technologies [39,40] to reduce CO_2 emissions and control global warming [41]. Hence, biomass based carbon adsorbents are excellent renewable materials that could be used to capture CO_2 from coal fired power plants.

3.8. Cost estimation

From cost estimation analysis with respect to per kg production, it is observed that the synthesised ACs are cheaper and comparable to the others commercially available. An amount of 1.93 US$ is calculated for the production of per kg of AC as shown in Table 5, while the amount of commercially available AC is in the range of 2–5 US$ per kg [42]. In literature, the synthesised ACs from the peels of *Artocarpus integer* fruit following the steam activation method were estimated to be cost-effective adsorbents (1.67 US$ per kg) [42], but these carbons were not evaluated for their CO_2 uptake potentials. Furthermore, the cost estimation analysis was carried out by following the summation of sample per kg cost of different components [42].

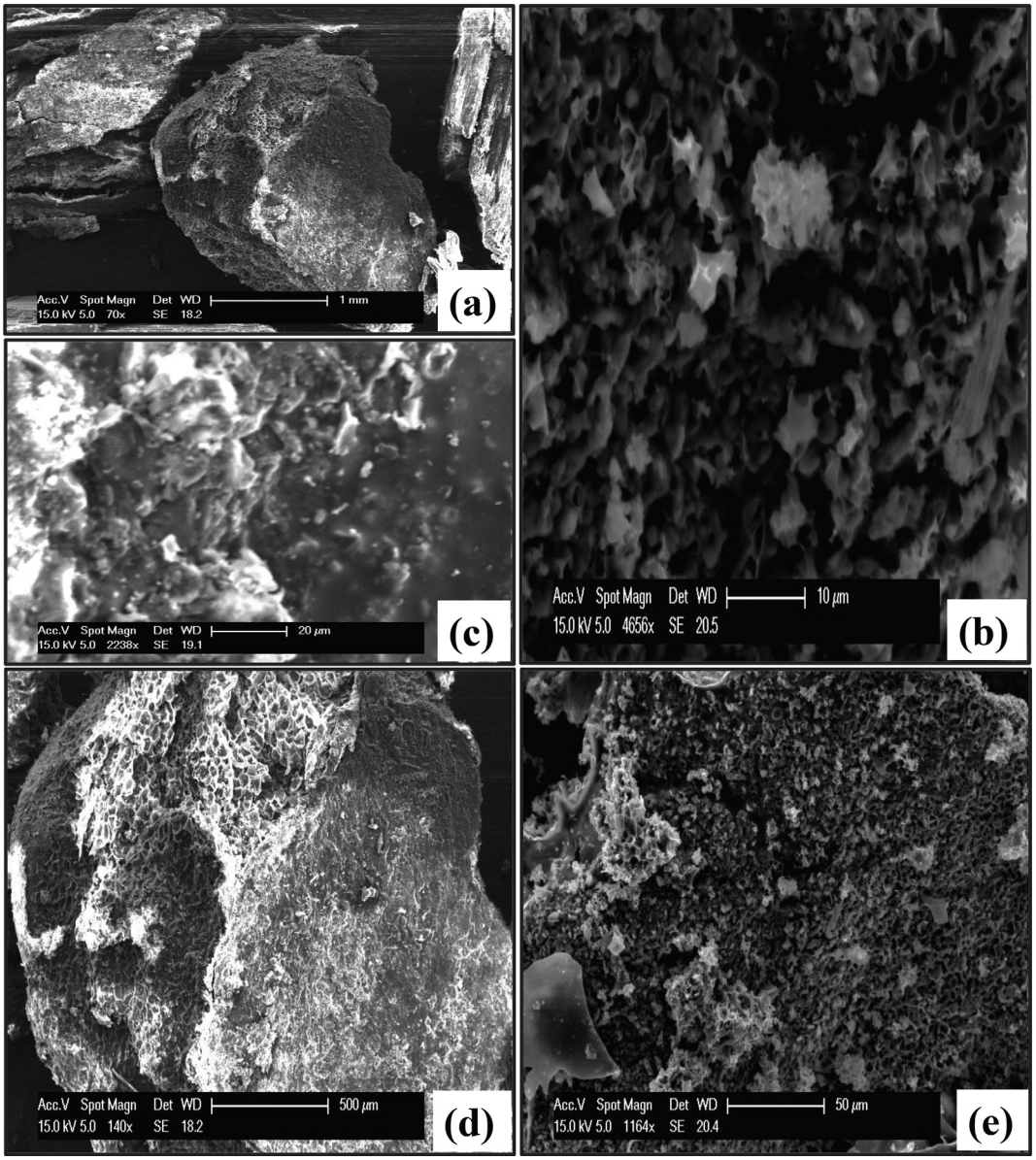

Fig. 13. SEM analysis of pine wood derived non-activated; PW (a, c and d), and activated carbons; PWK1 (b and e).

Table 4
CO_2 uptake rate of synthesised adsorbents.

ACs	Uptake in 1 h	Uptake in first 120 s	% CO_2 uptake in first 120 s
NSK1	2.71	1.55	57.30
NSK2	2.57	1.35	52.67
NSK3	3.23	1.34	41.64
NSK4	2.90	1.48	50.91
PNK1	3.18	2.80	88.05
PNK2	3.06	2.77	90.38
PNK3	3.92	2.38	60.76
PNK4	2.54	1.04	41.11
PWK1	3.49	3.01	86.21
PWK2	3.24	3.06	94.49
PWK3	2.84	2.00	70.49
PWK4	2.53	1.76	69.66

**CO_2 adsorption (over N_2 balance).

Table 5
Production cost estimation for ACs with KOH activation.

Components	US$/kg
KOH	0.38
Distilled water	0.50
Nitrogen gas	0.20
Power consumption	0.80
Transportation	0.05
Total	1.93

4. Conclusions

Detailed screening and development of adsorbents/ACs from diverse biomass residues that are cheap, low cost, sustainable, green agricultural waste, easily available and CO_2 neutral materials is carried out. This synthesis of ACs from biomass precursors will not only overcome the global warming issue but would also minimise the problems of land space covered by the selected biomass residues.

- TGA and BET analyses demonstrate that the adsorption capacities of different ACs are as; 3.23 > 2.90 > 2.71 > 2.57, 3.92 > 3.18 > 3.06 > 2.54 and 3.49 > 3.24 > 2.84 > 2.53 mmol/g for

NSK3 > NSK4 > NSK1 > NSK2, PNK3 > PNK1 > PNK2 > PNK4 and PWK1 > PWK2 > PWK3 > PWK4 respectively. Among all these the highest CO_2 (3.92 mmol/g) is noticed with PNK3 AC that is peanut shell derived.

- N_2 adsorption isotherms show Type I isotherm for NSK1, PNK3, PNK4, PWK1 and PWK2 and Type II isotherm for NSK3.
- Bimodal pore structure analyses verify the Type I and Type II N_2 sorption isotherms results.
- Peaks in the region < 50 nm confirm that mostly adsorbents' surface comprised of micro and mesopores.
- The catalytic KOH mechanistic approach and the resultant aromatization and gasification reactions are in accordance with FTIR peaks in region (808–893 cm^{-1}) and verified from SEM images.
- Characteristic XRD peaks of 2θ = 22-25° and 43° in case of non-activated precursors are developed into sharp ones for ACs.
- Cost estimation calculation showed the developed ACs are cheaper in comparison to commercially available ones.
- Future research could be directed towards soft woody biomass residues because they yield relatively more porous adsorbents upon activation with KOH than hard woody biomass.

CRediT authorship contribution statement

Farooq Sher: Conceptualization, Methodology, Software, Validation, Writing - review & editing, Supervision. **Sania Zafar Iqbal:** Data curation, Software, Visualization, Writing - original draft. **Shaima Albazzaz:** Writing. **Usman Ali:** Writing, Software, Validation. **Daniela Andresa Mortari:** Writing, Investigation, Validation. **Tazien Rashid:** Writing, Software, Investigation, Validation.

Declaration of Competing Interest

The authors declare that they have no known competing financial interests or personal relationships that could have appeared to influence the work reported in this paper.

Acknowledgement

The authors are thankful to the Higher Education Commission of Pakistan for the financial support to carry on this research.

Appendix A. Supplementary data

Supplementary data to this article can be found online at https://doi.org/10.1016/j.fuel.2020.118506.

References

[1] Li J, et al. Selective preparation of biomass-derived porous carbon with controllable pore sizes toward highly efficient CO2 capture. Chem Eng J 2019;360:250–9.
[2] Sher F, et al. Thermal and kinetic analysis of diverse biomass fuels under different reaction environment: A way forward to renewable energy sources. Energy Convers Manage 2020;203:112266.
[3] Li B, et al. Advances in CO2 capture technology: A patent review. Appl Energy 2013;102:1439–47.
[4] Liu X, et al. Potassium and zeolitic structure modified ultra-microporous adsorbent materials from a renewable feedstock with favorable surface chemistry for co2 capture. ACS Appl Mater Interfaces 2017;9(32):26826–39.
[5] Sher F, et al. Oxy-fuel combustion study of biomass fuels in a 20 kW th fluidized bed combustor. Fuel 2018;215:778–86.
[6] Sher F, et al. Experimental investigation of woody and non-woody biomass combustion in a bubbling fluidised bed combustor focusing on gaseous emissions and temperature profiles. Energy 2017;141:2069–80.
[7] Hai IU, et al., Experimental investigation of tar arresting techniques and their evaluation for product syngas cleaning from bubbling fluidized bed gasifier. 2019. 240: p. 118239.
[8] Figueroa JD, et al. Advances in CO_2 capture technology—The US Department of Energy's Carbon Sequestration Program. Int J Greenhouse Gas Control 2008;2(1):9–20.
[9] Coninck HD, et al. IPCC special report on carbon dioxide capture and storage. Intergovernmental Panel on. Clim Change 2005.
[10] Wang M, et al. Post-combustion CO2 capture with chemical absorption: a state-of-the-art review. Chem Eng Res Des 2011;89(9):1609–24.
[11] Hai IU et al., Assessment of biomass energy potential for SRC willow woodchips in a pilot scale bubbling fluidized bed gasifier. 2019. 258: p. 116143.
[12] Ao W, et al. Microwave assisted preparation of activated carbon from biomass: A review. Renew Sustain Energy Rev 2018;92:958–79.
[13] Djilani C, et al. Adsorption of dyes on activated carbon prepared from apricot stones and commercial activated carbon. J Taiwan Inst Chem Eng 2015;53:112–21.
[14] Hazzaa R, Hussein M. Adsorption of cationic dye from aqueous solution onto activated carbon prepared from olive stones. Environ Technol Innov 2015;4:36–51.
[15] Nowicki P, Kazmierczak J, Pietrzak R. Comparison of physicochemical and sorption properties of activated carbons prepared by physical and chemical activation of cherry stones. Powder Technol 2015;269:312–9.
[16] Jimenez-Cordero D, et al. Preparation of granular activated carbons from grape seeds by cycles of liquid phase oxidation and thermal desorption. Fuel Process Technol 2014;118:148–55.
[17] Ello AS, et al. Coconut shell-based microporous carbons for CO2 capture. Microporous Mesoporous Mater 2013;180:280–3.
[18] Tay T, Ucar S, Karagöz S. Preparation and characterization of activated carbon from waste biomass. J Hazard Mater 2009;165(1–3):481–5.
[19] Wahby A, et al. High-surface-area carbon molecular sieves for selective CO2 adsorption. ChemSusChem 2010;3(8):974–81.
[20] Tiwari D, Bhunia H, Bajpai PK. Adsorption of CO2 on KOH activated, N-enriched carbon derived from urea formaldehyde resin: kinetics, isotherm and thermodynamic studies. Appl Surf Sci 2018;439:760–71.
[21] Jiang L, et al. Post-combustion CO2 capture from a natural gas combined cycle power plant using activated carbon adsorption. Appl Energy 2019;245:1–15.
[22] Liu J, et al. Spherical potassium intercalated activated carbon beads for pulverised fuel CO2 post-combustion capture. Carbon 2015;94:243–55.
[23] Sait HH, et al. Pyrolysis and combustion kinetics of date palm biomass using thermogravimetric analysis. Bioresour Technol 2012;118:382–9.
[24] Lin G, et al. KOH activation of biomass-derived nitrogen-doped carbons for supercapacitor and electrocatalytic oxygen reduction. Electrochim Acta 2018;261:49–57.
[25] Hirst E, Taylor A, Mokaya R. A simple flash carbonization route for conversion of biomass to porous carbons with high CO2 storage capacity. J Mater Chem A 2018.
[26] Yakout S, El-Deen GS. Characterization of activated carbon prepared by phosphoric acid activation of olive stones. Arab J Chem 2016;9:S1155–62.
[27] Sun N, et al. Surface-modified spherical activated carbon materials for pre-combustion carbon dioxide capture. RSC Adv 2015;5(42):33681–90.
[28] Singh G, et al. Single step synthesis of activated bio-carbons with a high surface area and their excellent CO2 adsorption capacity. Carbon 2017;116:448–55.
[29] Presser V, et al. Effect of pore size on carbon dioxide sorption by carbide derived carbon. Energy Environ Sci 2011;4(8):3059–66.
[30] Rashidi NA, Yusup S. An overview of activated carbons utilization for the post-combustion carbon dioxide capture. J CO_2 Util 2016;13:1–16.
[31] Li M, Xiao R. Preparation of a dual pore structure activated carbon from rice husk char as an adsorbent for CO2 capture. Fuel Process Technol 2019;186:35–9.
[32] Liu X, et al. Developing hierarchically ultra-micro/mesoporous biocarbons for highly selective carbon dioxide adsorption. Chem Eng J 2019;361:199–208.
[33] Güleç F, Sher F, Karaduman A. Catalytic performance of Cu-and Zr-modified beta zeolite catalysts in the methylation of 2-methylnaphthalene. Pet Sci 2019;16(1):161–72.
[34] Wang J, Kaskel S. KOH activation of carbon-based materials for energy storage. J Mater Chem 2012;22(45):23710–25.
[35] Wang K, et al. Promising biomass-based activated carbons derived from willow catkins for high performance supercapacitors. Electrochim Acta 2015;166:1–11.
[36] Cuce E, et al. Strategies for ideal indoor environments towards low/zero carbon buildings through a biomimetic approach. Int J Ambient Energy 2019;40(1):86–95.
[37] Zhang Y, et al. Simulation of particle mixing and separation in multi-component fluidized bed using Eulerian-Eulerian method: a review. Int J Chem Reactor Eng 2019;17(11).
[38] Al-Juboori O, et al. The effect of variable operating parameters for hydrocarbon fuel formation from CO2 by molten salts electrolysis. J CO_2 Util 2020;40:101193.
[39] Al-Shara NK, et al. Electrochemical study of different membrane materials for the fabrication of stable, reproducible and reusable reference electrode. J Energy Chem 2020;49:33–41.
[40] Cuce E, et al. Sustainable ventilation strategies in buildings: CFD research. Sustain Energy Technol Assess 2019;36:100540.
[41] Hassan MHA, et al. Kinetic and thermodynamic evaluation of effective combined promoters for CO2 hydrate formation. J Nat Gas Sci Eng 2020:103313.
[42] Selvaraju G, Bakar NKA. Production of a new industrially viable green-activated carbon from Artocarpus integer fruit processing waste and evaluation of its chemical, morphological and adsorption properties. J Cleaner Prod 2017;141:989–99.